Two-site realization of the Davydov model in a finite size lattice: A time-convolutionless master equation approach

Vincent Pouthier*
Institut UTINAM, UMR CNRS 6213, Université de Franche-Comté, 25030 Besançon cedex, France
(Received 8 March 2007; published 21 June 2007)

A two-site realization of the Davydov model is introduced to study the energy flow between two amide-I modes embedded in a finite size lattice of hydrogen-bounded peptide units. The non-Markovian nature of the energy transfer is addressed by using a time convolutionless master equation for the population difference of quanta between the two sites of the dimer. It is shown that both the lattice size and the dimer position discriminate between two dynamical regimes. For specific values of these parameters, the population difference shows damped oscillations. It decreases exponentially and rapidly vanishes, which indicates that the equilibrium corresponds to a uniform energy distribution over the two sites of the dimer. By contrast, for other specific values of the lattice size and dimer position, a slowdown of the decoherence takes place. The population difference does not decay exponentially but evolves by steps during which the damping of the oscillations is very small. In addition, the occurrence of revivals characterizing an amplification of the coherence over a finite time scale is observed. Nevertheless, both the decoherence slowdown and the revivals are limited by pure dephasing so that the population difference finally vanishes, but after a rather large coherent time.

DOI: 10.1103/PhysRevE.75.061910 PACS number(s): 87.10.+e, 71.38.Ht, 63.22.+m, 05.60.Gg

I. INTRODUCTION

Since the seminal works of Davydov and co-workers [1] on the energy transfer in proteins, both theoretical and experimental evidences suggest that vibrational energy flow in α-helices may result from a polaron mechanism [2–14]. In such a molecular lattice, the energy flow is mediated by the high frequency vibration of each peptide group, namely the amide-I mode (CO) or the amide-A mode (NH), which delocalizes along the helix leading to the occurrence of vibrational excitons called vibrons. The polaron formation originates in the strong coupling between the vibrons and the phonons of the helix connected to the external motions of the residues. Since the vibron bandwidth is lower than the phonon cutoff frequency, the quantum behavior of the phonons plays a crucial role and the nonadiabatic strong coupling regime is reached. The creation of a vibron is thus accompanied by a virtual cloud of phonons describing a localized lattice distortion which follows instantaneously the vibron. The vibron dressed by the lattice distortion forms the small polaron.

The dressing mechanism results from a Lang-Firsov transformation [15] which is not exact due to the delocalized nature of the vibron. A rather weak coupling between the polaron and the phonons remains. It is responsible for dissipation and leads to incoherent diffusion. In that context, the transport properties of small polarons have been extensively studied during the last three decades (see for instance Refs. [16–23]). Most of these works were applied to lattices with translational invariance in which the phonons form a thermal bath. The transport was addressed within a projector method [24–26] to derive a generalized master equation (GME) for the polaron reduced density matrix. This equation involves the time convolution between the density matrix and the memory kernel which characterizes the history of the coupling. Because the correlation time of the phonon bath is usually smaller than the typical time for the free polaron evolution, the memory kernel vanishes rapidly so that the Markov approximation can be used to define a simplified GME.

Nevertheless, most proteins have compact and globular shapes due to frequent reversals of the direction of their polypeptide chains [27]. The analysis of the 3D structures of numerous proteins has revealed that they involve a set of secondary structures, such as α-helix and β-sheet, connected to each other by common structural elements called β-turn loop. It has been shown, form the Brookhaven Protein Data Bank (PDB), that helices containing from three to 15 residues are the most abundant in nature indicating that most proteins involve rather small helices [28].

Therefore, the fundamental question arises whether the finite size of the helix modifies the polaron transport properties. Indeed, in a finite size lattice the number of phonon modes is drastically reduced. The corresponding spectrum exhibits a discrete nature so that we expect the occurrence of time recurrences in the memory kernel. As pointed out by Pereverzev and Bittner [29], these recurrences will prevent the kernel to vanish in the long time limit so that non-markovian effects are expected to affect the polaron dynamics. Although the standard projector method provides an exact treatment of non-Markovian effects, the GME cannot be solved easily due to the presence of a time convolution. To overcome this difficulty, a new approach has been elaborated by renormalizing the memory kernel, i.e., by performing a different resummation of the perturbation series. This method, called time-convolutionless master equation (TCLME), allows a systematic analysis of the non-Markovian quantum dynamics of open systems (see for instance Refs. [29–35]). It presents the advantage of being local in time and yields an evolution equation for the reduced density matrix independent on all the history of the coupling.

*vincent.pouthier@univ-fcomte.fr

In addition, it has been shown that to second order in the coupling strength, the TCLME gives a better approximation to the exact solution than the standard GME.

In that context, the aim of the present paper is to address a comprehensive theory to describe the influence of the lattice size onto the polaron dynamics. For that purpose, we consider a system formed by a two-site realization of the Davydov model involving two nearest neighbor amide-I modes embedded in an finite size lattice. Although this model is rather unrealistic to describe the vibrational dynamics of a real α-helix, it provides a rather simple approach to clearly understand the modification of the dressing mechanism due to the finite size of the lattice. A more realistic model involving several amide-I modes embedded in a finite size lattice will be presented in forthcoming works.

The paper is organized as follows. In Sec. II, the two-site Davydov model is described and the key observables required to study the transport properties are introduced. In Sec. III, the polaron-phonon coupling is treated and the TCLME is established. This equation is solved numerically in Sec. IV where a detailed analysis of the energy transfer between the two sites is performed. Finally, these results are discussed and interpreted in Sec. V.

II. DESCRIPTION OF THE SYSTEM

A. Model and Hamiltonians

Within the two-site realization of the Davydov model, we consider a finite size lattice whose N sites $n=1,\ldots,N$ contain the peptide groups. In this lattice, two amide-I modes are located on the sites n_0 and $n_1=n_0+1$. If $|i\rangle$ denotes the first vibrational excited state of the n_ith amide-I mode, the vibron Hamiltonian H_v is expressed as (using the convention $\hbar=1$),

$$H_v = \sum_{i=0,1} \omega_0 |i\rangle\langle i| + \Phi(|0\rangle\langle 1| + |0\rangle\langle 1|), \tag{1}$$

where ω_0 is the internal frequency of each mode and Φ represents the hopping constant between the two sites.

This dimer interacts with the phonons of the lattice describing the external motions of the peptide groups. To mimic the fact that a real α-helix in a globular protein is embedded in its protein matrix, we assume that the peptide groups are confined between two potential wells. As a result, the phonon Hamiltonian is written as

$$H_p = \sum_{n=1}^{N} \frac{p_n^2}{2M} + \sum_{n=1}^{N-1} \frac{W}{2}(u_{n+1}-u_n)^2 + \frac{W}{2}(u_1^2+u_N^2), \tag{2}$$

where M is the mass of each peptide group whose displacement and momentum are u_n and p_n, respectively, and where W is the lateral force constant between nearest neighbor groups. The last two terms in Eq. (2) account for the coupling between the side groups $n=1$ and $n=N$ and the protein matrix supposed to be rigid. To simplify our discussion, these couplings are characterized by the force constant W so that the lattice is equivalent to a 1D chain with fixed boundary conditions.

In a finite size lattice, the phonons do not correspond to Bloch waves with well defined wave vectors. The sides of the lattice lead to reflections so that the true eigenstates are superimpositions of incident and reflected plane waves. A stationary regime takes place and the phonon eigenstates correspond to N normal modes with quantized wave vectors $q_p=p\pi/L$, with $p=1,\ldots,N$ and $L=N+1$. The corresponding frequencies are defined as $\Omega_p=\Omega_c \sin(p\pi/2L)$ where $\Omega_c=\sqrt{4W/M}$. Within this normal mode representation, the phonon Hamiltonian [Eq. (2)] is rewritten in terms of the standard phonon operators $a_p^\dagger$ and a_p as

$$H_p = \sum_{p=1}^{N} \Omega_p (a_p^\dagger a_p + 1/2). \tag{3}$$

According to the Davydov model, the phonon bath yields random fluctuations of the internal frequency of each amide-I mode which depends linearly on the phonon coordinates. Therefore, within the normal mode representation, the vibron-phonon coupling Hamiltonian is written as

$$\Delta H_{\mathrm{vp}} = \sum_{p,i} \Delta_{p,i}(a_p^\dagger + a_p)|i\rangle\langle i|, \tag{4}$$

where the coupling constant $\Delta_{p,i}$ is expressed as

$$\Delta_{p,i} = \sqrt{\frac{2}{L}}\Delta_0 \frac{\cos\left(\frac{p\pi n_i}{L}\right)\sin\left(\frac{p\pi}{L}\right)}{\sqrt{\sin\left(\frac{p\pi}{2L}\right)}}. \tag{5}$$

In Eq. (5), Δ_0 is defined in terms of the coupling parameter χ introduced in the original Davydov model as $\Delta_0=\chi(\hbar^2 MW)^{-1/4}$ ($\hbar$ has been reintroduced to avoid confusion).

At this step, let us mention the formal resemblance between our model Hamiltonian and the spin boson model describing a two-level system coupled with a bath of bosonic excitations (see, for instance, Refs. [26,32,33,36–38]). Indeed, in terms of the standard Pauli matrices S_x, S_y and S_z, the full Hamiltonian $H=H_v+H_p+\Delta H_{\mathrm{vp}}$ can be rewritten as

$$H = \omega_0 \mathbf{1} + \Phi S_x + H_p + \sum_{p=1}^{N} \frac{\Delta_{p,0}+\Delta_{p,1}}{2}(a_p^\dagger + a_p) + S_z \sum_{p=1}^{N} \frac{\Delta_{p,0}-\Delta_{p,1}}{2}(a_p^\dagger + a_p). \tag{6}$$

Equation (6) reveals two main differences between our model and the spin boson model. Indeed, the standard spin boson model involves a rather large number of harmonic oscillators so that the coupling between the bosons and the two-level system is described by the so-called continuous coupling distribution [26]. By contrast, in our case, the bath involves a reduced set of modes due to the finite size of the lattice. In addition each bath mode experiences a linear perturbation so that its eigenstates correspond to coherent states instead of the standard number states.

The vibron-phonon dynamics is thus described by the full Hamiltonian H. Although it yields a rather simple model for the dimer dynamics, it cannot be solved exactly due to the nonlinear vibron-phonon coupling. The following section is thus devoted to its simplification.

B. Polaron point of view

To partially remove the coupling ΔH_{vp} in the nonadiabatic strong coupling regime, a Lang-Firsov transformation [15] is applied to the full Hamiltonian H (see, for instance, Refs. [5–10,23]). By using a mean field procedure, the resulting Hamiltonian is expressed as the sum of three separated contributions as $\hat{H}=H_{\mathrm{po}}+H_p+\Delta H$. The polaron Hamiltonian H_{po} is written as

$$H_{\mathrm{po}}=\sum_{i=0,1}[\omega_0-\epsilon(N)]|i\rangle\langle i|+\hat{\Phi}(|0\rangle\langle 1|+|1\rangle\langle 0|), \quad (7)$$

where $\epsilon(N)=\Sigma_p\Delta_{p,i}^2/\Omega_p$. The effective hopping constant $\hat{\Phi}=\Phi\langle\Theta_0^+\Theta_1\rangle_p$ is defined as the thermal average over the phonon bath $\langle\cdots\rangle_p$ of the product of the so-called dressing operator

$$\Theta_i=\exp\left[-\sum_p\left(\frac{\Delta_{p,i}}{\Omega_p}(a_p^\dagger-a_p)\right)\right]. \quad (8)$$

In this point of view, the state $|i\rangle$ defines a small polaron, i.e., a vibrational excitation of the n_ith amide-I mode dressed by a lattice distortion. The dressing prevents the delocalization of the polaron whose effective hopping constant $\hat{\Phi}$ is smaller than the bare constant Φ. At biological temperature, we have verified that $\hat{\Phi}$ does not depend on both the dimer position and the lattice size and it is equal to the constant characterizing a dimer embedded in an infinite lattice. By contrast, at low temperature, $\hat{\Phi}$ exhibits weak inhomogeneities since it slightly increases when the dimer is located close to a lattice side. In the same way, $\epsilon(N)$ is independent on the dimer position. However, it increases with the lattice size to reach $\epsilon(\infty)=2\Delta_0^2/\Omega_c$ when N tends to infinity. This value, denoted E_B in the following of the text, defines the so-called small polaron binding energy.

From Eq. (7), the polaronic eigenstates are delocalized over the two sites of the dimer. They correspond to a symmetric and to an antisymmetric superimpositions of the localized states $|i\rangle$ written as

$$|\pm\rangle=\frac{1}{\sqrt{2}}(|0\rangle\pm|1\rangle). \quad (9)$$

The corresponding eigenenergies are thus defined as $\omega_\pm=\omega_0-\epsilon(N)\pm\hat{\Phi}$.

Finally, a polaron-phonon coupling remains because of the nonvanishing value of the hopping constant Φ. The corresponding Hamiltonian is written as

$$\Delta H=V_{01}|0\rangle\langle 1|+V_{10}|1\rangle\langle 0|, \quad (10)$$

where $V_{ij}=\Phi(\Theta_i^\dagger\Theta_j-\langle\Theta_i^\dagger\Theta_j\rangle_p)$. This coupling describes a random modulation of the polaron hopping constant which depends on the phonon coordinates in a highly nonlinear way. It favors a polaron transition between the two sites of the dimer mediated by the emission or the absorption of phonons. Note that in the eigenstate basis $\{|+\rangle,|-\rangle\}$, this coupling Hamiltonian has both diagonal and nondiagonal elements as

$$\Delta H=\frac{1}{2}\begin{pmatrix}V_{01}+V_{10} & -V_{01}+V_{10}\\ V_{01}-V_{10} & -V_{01}-V_{10}\end{pmatrix}. \quad (11)$$

Although a coupling remains, the polaron-phonon interaction has been strongly reduced within the polaron point of view. A standard perturbation theory can thus be applied to describe the dynamics of the system, as shown in the next sections.

Note that in terms of the standard Pauli matrices, the full Hamiltonian $\hat{H}$ can be rewritten as

$$\hat{H}=[\omega_0-\epsilon(N)]+\hat{\Phi}S_x+H_p+\left(\frac{V_{01}}{2}S_+ +\frac{V_{10}}{2}S_-\right), \quad (12)$$

where $S_\pm=S_x\pm iS_y$. In the polaron point of view, the interaction between the spin and the bosons is defined in terms of the dressing operators. It is thus strongly nonlinear in a marked contrast with the standard spin boson model in which the coupling depends linearly on the boson coordinates.

C. Polaron reduced density matrix

A complete understanding of the vibrational energy flow is obtained from the knowledge of the reduced density matrix whose diagonal elements yield the population of the undressed states. Since the vibron number is conserved under the Lang-Firsov transformation, the population of the undressed states is equal to that of the dressed states. Therefore, the information that is desired is contained in the diagonal elements of the reduced density matrix expressed in the polaron point of view.

By performing an average over the phonon bath, this matrix is written as $\sigma(t)=Tr_p[\exp(-i\hat{H}t)\hat{\rho}\exp(i\hat{H}t)]$. The time evolution corresponds to an Heisenberg representation with respect to $\hat{H}$ and the initial conditions are specified by the transformed density matrix $\hat{\rho}$. Without any perturbation, the system is in thermal equilibrium at the biological temperature T. Therefore, since $\hbar\omega_0\gg k_BT$, the vibrons cannot be thermally excited at biological temperature. This is no longer the case for the phonons ($\Omega_c\ll\omega_0$) whose eigenstates are not well defined. A statistical average is thus required by using the Boltzmann distribution ρ_p for the phonon density matrix. Therefore, the energy transfer between the two amide-I results from the excitation of the dimer in a state out of equilibrium. For that reason, we suppose that a vibron is initially created on the site n_0. The initial density matrix is thus written as the tensorial product $\rho=\rho_v\otimes\rho_p$, where $\rho_v=|0\rangle\langle 0|$. However, under the Lang-Firsov transformation, the phonon density matrix is modified since the creation of a vibron yields a polaron accompanied by a lattice distortion. Nevertheless, it will be assumed that the lattice is fully relaxed before the polaron begins to move so that $\hat{\rho}\approx\rho$ [22].

In that context, the population of the dressed state $|i\rangle$ is given by the diagonal element of the reduced density matrix $P_i(t)=\sigma_{ii}(t)$. Since the population is conserved, i.e., $P_0(t)+P_1(t)=1$, only the population difference is required to have a complete description of the energy transfer. It is defined as

$$P(t) = \sigma_{00}(t) - \sigma_{11}(t) \tag{13}$$

with $P(0)=1$. Although this approach provides a spatial view of the energy transfer, the same information can be extracted from the representation of the reduced density matrix in the polaron eigenstates $|\pm\rangle$. In that case, $P(t)$ is a measure of the coherence between the eigenstates as

$$P(t) = 2\ \mathrm{Re}\ \sigma_{+-}(t). \tag{14}$$

These features clearly show that the reduced density matrix is the central object of the present study. The following section is thus devoted to the derivation of a TCLME to study its evolution. To proceed, the representation in the eigenstates will be used because it simplifies the calculations and offers a clear meaning of the physical processes.

III. TIME-CONVOLUTIONLESS MASTER EQUATION

To determine the time evolution of the reduced density matrix, most of the projector methods involve a partial trace over the phonon bath of the full time dependent density matrix. The well-known projector $\mathcal{P}\ldots=\rho_p Tr_p\ldots$ is introduced and it is applied to determine the behavior of the evolution operator $\mathcal{U}(t)=\exp(-i\mathcal{L}t)$, where $\mathcal{L}=[\hat{H},\ldots]$ is the Liouvillian associated to $\hat{H}$. This procedure was called the Schrödinger picture formalism by Uchiyama and Shibata [31]. In the present work, we use the Heisenberg picture in which the reduced density matrix is expressed in terms of the Hermitian conjugate evolution operator as

$$\sigma_{\alpha\beta}(t) = Tr_v[\rho_v \mathcal{U}_P^\dagger(t)|\beta\rangle\langle\alpha|], \tag{15}$$

where $\alpha,\beta=\pm$ and $\mathcal{U}_P^\dagger(t)=Pe^{i\mathcal{L}t}P$ is a projection according to the projector $P\ldots=Tr_p[\rho_p\ldots]$ which denotes an average over the phonon bath.

The standard projector method of the TCLME approach is then used to characterize the time evolution of the superoperator $\mathcal{U}_P^\dagger(t)$. This procedure is detailed in Ref. [31] by using the interaction picture in which the coupling Hamiltonian is time dependent. Here, the projector method is directly applied on the time independent polaron-phonon interaction. Therefore, by performing a second order perturbation theory with respect to ΔH [Eq. (10)], it is straightforward to show that $\mathcal{U}_P^\dagger(t)$ satisfies the TCLME

$$\frac{\partial \mathcal{U}_P^\dagger(t)}{\partial t} = i\mathcal{U}_P^\dagger(t)[\mathcal{L}_{\mathrm{po}} + \delta\mathcal{L}(t)], \tag{16}$$

where

$$\delta\mathcal{L}(t) = i\int_0^t dt_1 \langle \mathcal{U}_0^\dagger(-t_1)\Delta\mathcal{L}\mathcal{U}_0^\dagger(t_1)\Delta\mathcal{L}\rangle_p. \tag{17}$$

In Eq. (17), $\Delta\mathcal{L}=[\Delta H,\ldots]$ and $\mathcal{U}_0^\dagger(t)=\exp(i\mathcal{L}_0 t)$ is expressed in terms of the unperturbed Liouvillian $\mathcal{L}_0=[H_{\mathrm{po}}+H_p,\ldots]$.

After some algebraic manipulations, the development of Eq. (16) can be performed to finally obtain the TCLME for the reduced polaron density matrix [Eq. (15)] as

$$\dot{\sigma}_{++}(t) = -W_{+-}(t)\sigma_{++}(t) + W_{-+}(t)\sigma_{--}(t),$$

$$\dot{\sigma}_{--}(t) = -W_{-+}(t)\sigma_{--}(t) + W_{+-}(t)\sigma_{++}(t),$$

$$\dot{\sigma'}_{+-}(t) = 2[\hat{\Phi}+\Delta(t)]\sigma''_{+-}(t) - [\Gamma^*(t)+W(t)]\sigma'_{+-}(t),$$

$$\dot{\sigma''}_{+-}(t) = -2\hat{\Phi}\sigma'_{+-}(t) - \Gamma^*(t)\sigma''_{+-}(t), \tag{18}$$

where $\sigma_{+-}(t)=\sigma'_{+-}(t)+i\sigma''_{+-}(t)=\sigma^*_{-+}(t)$. The dynamical parameters in Eq. (18) are defined as

$$W_{+-}(t) = \mathrm{Re}\int_0^t dt_1[C_+(t_1) - C_-(t_1)]e^{2i\hat{\Phi}t_1},$$

$$W_{-+}(t) = \mathrm{Re}\int_0^t dt_1[C_+(t_1) - C_-(t_1)]e^{-2i\hat{\Phi}t_1},$$

$$\Gamma^*(t) = 2\ \mathrm{Re}\int_0^t dt_1[C_+(t_1) + C_-(t_1)],$$

$$\Delta(t) = \mathrm{Re}\int_0^t dt_1[C_+(t_1) - C_-(t_1)]\sin(2\hat{\Phi}t_1),$$

$$W(t) = W_{+-}(t) + W_{-+}(t), \tag{19}$$

where $C_+(t)=\langle V_{01}(t)V_{10}(0)\rangle_p$ and $C_-(t)=\langle V_{01}(t)V_{01}(0)\rangle_p$ denote the correlation functions of the polaron-phonon coupling Hamiltonian. They are defined as

$$C_\pm(t) = \hat{\Phi}[e^{\pm[K(t)-iS(t)]} - 1], \tag{20}$$

where $K(t)$ and $S(t)$ are expressed in terms of $\delta\Delta_p=\Delta_{p0}-\Delta_{p1}$ as

$$K(t) = \sum_p \left(\frac{\delta\Delta_p}{\Omega_p}\right)^2 \coth\left(\frac{\omega_p}{2k_BT}\right)\cos(\Omega_p t),$$

$$S(t) = \sum_p \left(\frac{\delta\Delta_p}{\Omega_p}\right)^2 \sin(\Omega_p t). \tag{21}$$

The first two equations of the TCLME Eq. (18) describe the time evolution of the population of the dimer eigenstates. They appear as a generalized Pauli master equation with time dependent transition rates. By contrast, the last two equations govern the behavior of the coherence between the eigenstates. These four equations involve the dynamical parameters defined in Eq. (19) which account for the influence of the phonon bath. As shown in Eq. (11), this influence is twofold.

First, the nondiagonal elements of ΔH favor a coupling between $|+\rangle$ and $|-\rangle$ mediated by the exchange of phonons. Such a coupling induces incoherent transitions which modify the population of the eigenstates and which are characterized by the time dependent transition rates $W_{+-}(t)$ and $W_{-+}(t)$. According to the standard perturbation theory, $W_{+-}(t)$ $[W_{-+}(t)]$ is the time derivative of the probability $P_{+-}(t)$ $[P_{-+}(t)]$ to observe the dimer in $|-\rangle$ $(|+\rangle)$ at time t given that it was initially in $|+\rangle$ $(|-\rangle)$. As shown in Eq. (19), these rates are defined in terms of the integral of the product between

the correlation function of the non diagonal elements of ΔH and a phase factor $\exp(\pm 2i\hat{\Phi}t)$ describing the free evolution of the dimer. This product corresponds to the two time correlation function of an elementary transition amplitude which measures the memory of the dimer at time t of a transition realized at any time $t-t_1$ via the exchange of phonons.

The second influence of the phonon bath is described by the diagonal elements of ΔH which yield random fluctuations of the eigenenergies $\omega_{\pm}$. If the dimer state is written as a superimposition of $|+\rangle$ and $|-\rangle$, these fluctuations affect the phase relation between the eigenstates and drastically modify the coherent nature of the superimposition. They tend to destroy any quantum coherence and they characterize the so-called pure dephasing mechanism. Such a quantum decoherence is described by the parameter $\Gamma^*(t)$ which clearly appears as the time integral of the correlation function of the phase difference $\Delta H_{++}-\Delta H_{--}$. Note that, as shown by the occurrence of the parameter $W(t)$ in the third equation of Eq. (18), incoherent transitions mediated by phonon exchange also contribute to dephasing.

Finally, let us note that the polaron-phonon coupling is responsible for a dynamical shift of the Bohr frequency of the dimer. This shift is described by the parameter $\Delta(t)$ [Eq. (18)] which modifies the energy difference $2\hat{\Phi}=\omega_+-\omega_-$ between the two eigenstates.

Equation (18) allows us to derive a master equation for the population difference $P(t)$ [see Eqs. (13) and (14)]. However, $\sigma'_{+-}(t)$ and $\sigma''_{+-}(t)$ are coupled to each other which indicates that two equations are required to describe the time evolution of $P(t)$. This feature originates in the fact that both H_{po} and ΔH couple the populations and the coherences of the reduced density matrix expressed in the dressed basis. To account for this feature, let us introduce the coherence $J(t)=i[\sigma_{01}(t)-\sigma_{10}(t)]=2\sigma''_{+-}(t)$. Within these notations, $P(t)$ satisfies the following system of equations:

$$\dot{P}(t) = 2[\hat{\Phi} + \Delta(t)]J(t) - [\Gamma^*(t) + W(t)]P(t),$$

$$\dot{J}(t) = -2\hat{\Phi}P(t) - \Gamma^*(t)J(t). \tag{22}$$

The master equation (22) governs the energy flow between the two sites of the dimer. It depends on the three dynamical parameters $\Gamma^*(t)$, $W(t)$, and $\Delta(t)$ which strongly depend on the nature of the phonon modes and are thus very sensitive to the size of the lattice.

IV. NUMERICAL RESULTS

In this section, the numerical integration of the TCLME is performed within the fourth order Runge-Kutta method [39]. To proceed, typical values for the relevant parameters are used. The bare hopping constant is fixed to $\Phi=7$ cm^{-1} and the phonon cutoff frequency is equal to $\Omega_c=92$ cm^{-1}. However, the vibron-phonon coupling strength χ will be considered as a free parameter.

For a dimer located at the center of the lattice, the time evolution of the population difference is illustrated in Fig. 1 for $\chi=20$ pN (full line) and $\chi=30$ pN (dashed line). The

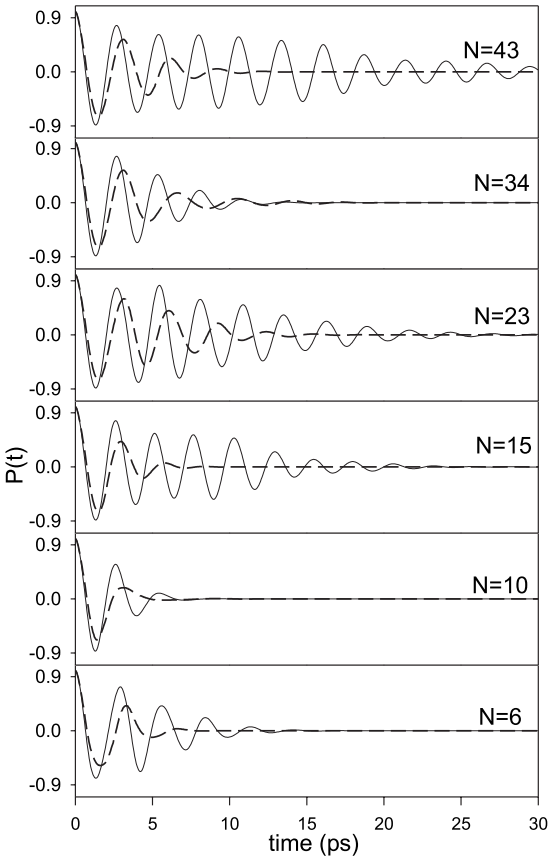

FIG. 1. Time evolution of the population difference for $\chi=20$ pN (full line) and $\chi=30$ pN (dashed line) for a dimer located at the center of lattice. The temperature is $T=300$ K. Six different values of the lattice size have been considered.

temperature is fixed to $T=300$ K and six different values of the lattice size have been considered. In a general way, $P(t)$ exhibits damped oscillations to finally vanish indicating that the equilibrium corresponds to a uniform energy distribution over the two sites of the dimer. Nevertheless, the time needed to reach the equilibrium, i.e., the so-called coherent time, strongly depends on both N and χ. Since the coupling with the phonons enhances the dissipation, the coherent time decreases with χ. However, its dependence on the lattice size is more surprising. For instance, for $\chi=20$ pN and for $N=6$ and 34, the coherent time takes intermediate values whereas it is drastically reduced when $N=10$. By contrast, for $N=15$, 23, and 43, $P(t)$ shows coherent oscillations over a significant timescale typically of about three times greater than the coherent time observed for $N=10$. Nevertheless, such a behavior depends on the coupling strength since for $\chi=30$ pN the larger coherent time is observed for $N=23$, only. However a short coherent time still remains for $N=10$. In addition, Fig. 1 shows that the dissipation does not lead to a strictly exponential damping. For instance, when $N=15$ and $\chi=20$ pN, $P(t)$ first decreases in the short time limit and then evolves almost without any damping until $t=10$ ps. Finally, it decays to reach the equilibrium. Similarly, for $N=43$, the amplitude of $P(t)$ is almost constant when time ranges between 5 and 15 ps. Then, it slightly decreases until t reaches 20 ps to develop again a time evolution with almost

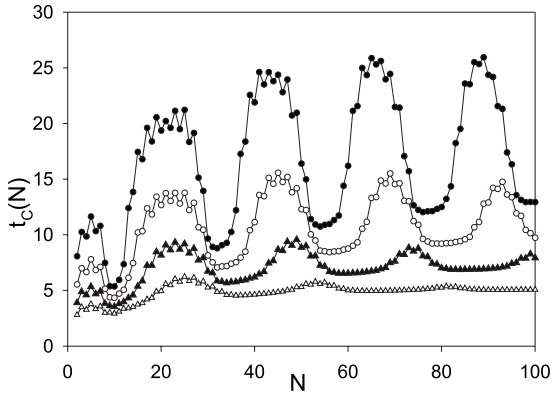

FIG. 2. Coherent time vs N for $n_0=N/2$ and for $T=200$ K and $\chi=20$ pN (full circles), $T=300$ K and $\chi=20$ pN (open circles), $T=200$ K and $\chi=30$ pN (full triangles), and $T=300$ K and $\chi=30$ pN (open triangles).

no damping until $t=30$ ps. Moreover, for $N=23$, the decay experienced by $P(t)$ in the short time limit is followed by an increase of its amplitude which reaches a maximum value around $t=5.5$ ps. This feature is a clear evidence for the occurrence of a coherence revival.

To clarify the influence of the lattice size, the qualitative behavior of the coherent time with respect to N is displayed in Fig. 2 for $T=200$ K and $\chi=20$ pN (full circles), $T=300$ K and $\chi=20$ pN (open circles), $T=200$ K and $\chi=30$ pN (full triangles), and $T=300$ K and $\chi=30$ pN (open triangles). This coherent time is defined as the area described by the curves $P^2(t)$ as

$$\frac{1}{t_c(N)} = 4\int_0^\infty dt\, P^2(t). \tag{23}$$

Figure 2 reveals the occurrence of specific domains which discriminates between large and short coherent times. For instance, for $T=200$ K and $\chi=20$ pN, short coherent times are observed when N is close to 10, 32, 54, and 76. By contrast, large coherent times occur when N is about 20, 42, 65, and 88. The same features are observed on the other curves. Nevertheless, the position of the domains is slightly shifted as both T and χ increase. Note that for a strong χ value and at high temperature, the coherent time becomes almost independent on the lattice size for large N values.

The time evolution of the rate $W(t)$ is illustrated in Fig. 3 for $T=300$ K and $\chi=20$ pN. Three values of the lattice size have been considered, i.e., $N=10$, $N=15$ and $N=23$, which characterize a short, an intermediate and a large coherent time, respectively. Whatever N, the rate varies almost periodically between positive and negative values. However, both the frequency and the amplitude of these variations strongly depend on the lattice size. When $N=10$, $W(t)$ typically behaves as a high amplitude sine function whose amplitude and period are about 9 cm^{-1} and 40 ps, respectively. Note that it does not exhibit a continuous nature but evolves by steps whose duration is about 1.1 ps in the short time limit. When $N=15$, the rate shows a rather similar behavior since it still alternates between positive and negative values

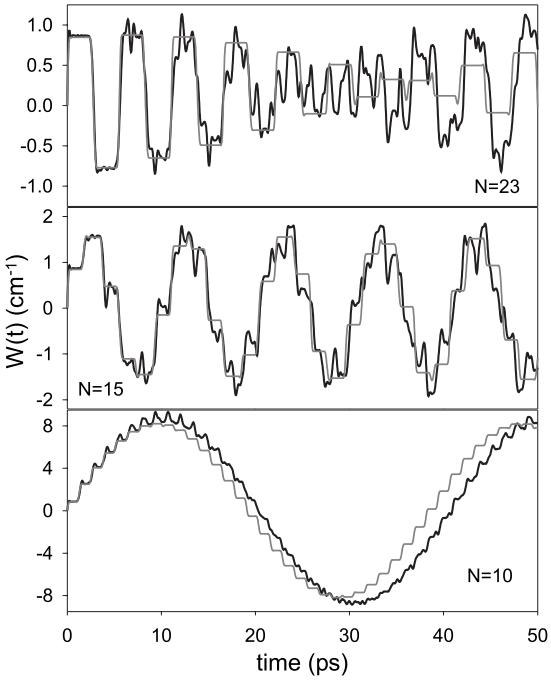

FIG. 3. Time evolution of the transition rate $W(t)$ for $n_0=N/2$, $T=300$ K, and $\chi=20$ pN and for $N=10$, $N=15$, and $N=23$. Gray lines represent theoretical calculations (see the text).

according to a sinelike function. However, the frequency of these variations has increased and the corresponding amplitude has been reduced to 1.5 cm^{-1}. In addition, the evolution by steps is more pronounced, the duration of each step being of about 1.5 ps. Finally, when $N=23$, the rate shows a series of positive and negative steps in the short time limit. Indeed, it rapidly increases to reach an almost constant value equal to 0.8 cm^{-1} over a time scale of about 2.5 ps. Then, the rate suddenly decreases to reach a negative value equal to -0.8 cm^{-1} over a similar time scale. Such a behavior basically remains until $t=20$ ps and finally disappears. However, it recurs in the long time limit for which a series of positive and negative steps reappears. Note that, in the very short time limit, the behavior of the rate is independent on the lattice size. The establishment of the first step is the same whatever the value of N. Nevertheless, as explained previously, its duration increases with N.

For the same set of parameters, the behavior of the pure dephasing constant is displayed in Fig. 4. In marked contrast with the transition rate, $\Gamma^*(t)$ is always positive. It increases with time but decreases with N. Although it seems to increase linearly with time, its short time behavior shown in the inset of Fig. 4 reveals that $\Gamma^*(t)$ increases by steps more or less well-defined.

As shown in Fig. 5 where $N=21$, the coherent time is also sensitive to the dimer position n_0. Note that the parameters are the same as those used in Fig. 2. Whatever both T and χ, the coherent time is maximum when the dimer is located in the middle of the lattice, i.e., when $n_0=10$ and 11. Then it decreases as n_0 is shifted to reach a minimum value when $n_0=5$ and 16. When $T=200$ K and $\chi=20$ pN, the value of the coherent time when $n_0=10$ is about three times greater than the coherent time for a dimer located on the site $n_0=5$.

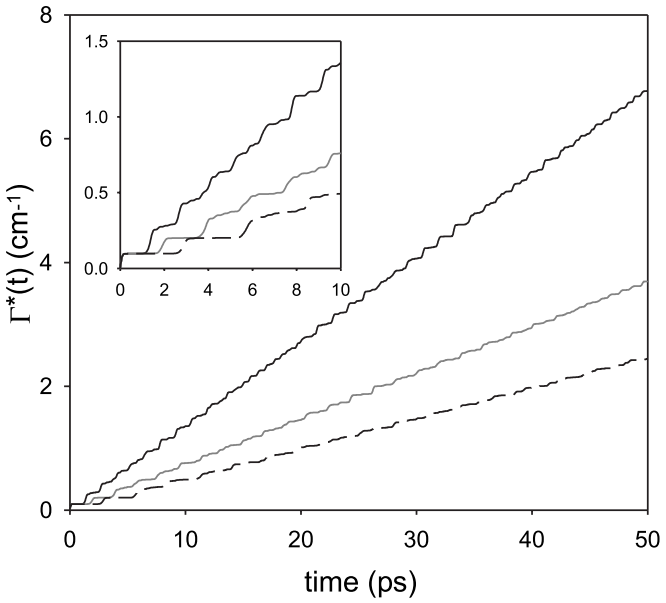

FIG. 4. Time evolution of the pure dephasing constant $\Gamma^*(t)$ for $n_0=N/2$, $T=300$ K, and $\chi=20$ pN and for $N=10$ (full line), $N=15$ (gray line), and $N=23$ (dashed line).

However, this ratio decreases with both the temperature and the strength of the coupling. For instance, it reduces to 1.5 when $T=300$ K and $\chi=30$ pN.

To illustrate the effect of the dimer position, the time evolution of the population difference is displayed in Fig. 6 for $n_0=10$ [Fig. 6(a)] and $n_0=5$ [Fig. 6(b)]. The parameters used are $T=200$ K and $\chi=20$ pN. When $n_0=5$, $P(t)$ rapidly vanishes after about 13 ps and it clearly shows an exponential decay. By contrast, when $n_0=10$, the coherent behavior of $P(t)$ survives until $t=40$ ps. As observed in Fig. 1 for specific N values, $P(t)$ does not decay exponentially. Indeed, a coherence revival occurs in the short time limit characterized by an enhancement of the population difference around $t=5$ ps. Then the two following oscillations show that $P(t)$ is almost constant until $t=10$ ps. These features indicate that a significant decay of $P(t)$ takes places only after 10 ps.

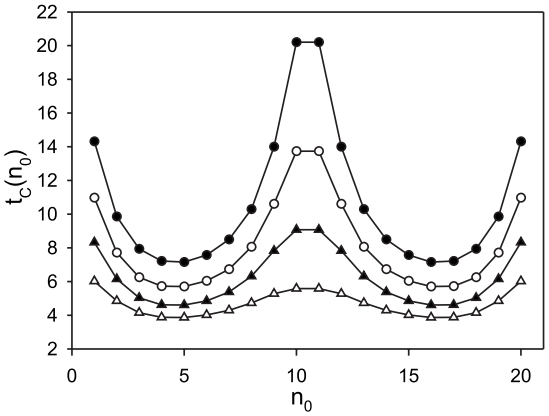

FIG. 5. Coherent time vs n_0 for $N=21$ and for $T=200$ K and $\chi=20$ pN (full circles), $T=300$ K and $\chi=20$ pN (open circles), $T=200$ K and $\chi=30$ pN (full triangles), and $T=300$ K and $\chi=30$ pN (open triangles).

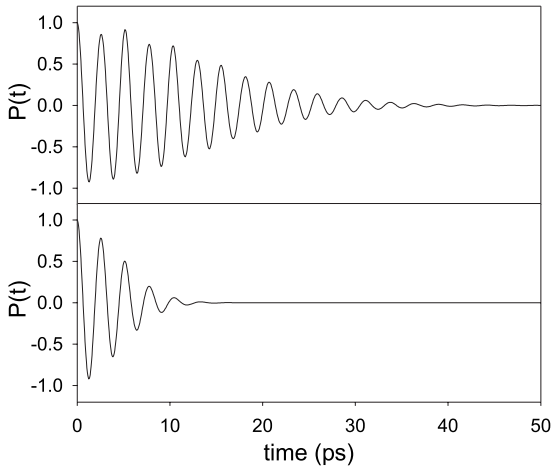

FIG. 6. Time evolution of the population difference for (a) $n_0=10$ and (b) $n_0=5$. The parameters used are $T=200$ K, $\chi=20$ pN, and $N=21$.

To understand this surprising effect, the time evolution of both $W(t)$ and $\Gamma^*(t)$ is shown in Fig. 7 for $n_0=10$ (full line) and $n_0=5$ (dashed line). When $n_0=10$, $W(t)$ exhibits a series of steps alternatively positive and negative whose amplitude is about 0.6 cm^{-1}. The shape of $W(t)$ is well defined in the short time limit with a step duration equal to 2.6 ps. However, as time increases high frequency low amplitude modulations occur which slightly modify the shape of $W(t)$. In a marked contrast, when $n_0=5$, the rate drastically increases and it takes positive value, only, over the time scale represented on the figure. Its exhibits two kinds of steps with different durations. In the very short time limit, the value of the rate is equal to that of the rate for $n_0=10$ until $t=1.0$ ps. Then, it increases to reach 1.2 cm^{-1} until $t=3.7$ ps to finally continue to increase. As shown in Fig. 7(b), $\Gamma^*(t)$ is not so sensitive to the dimer position. In the short time limit, it

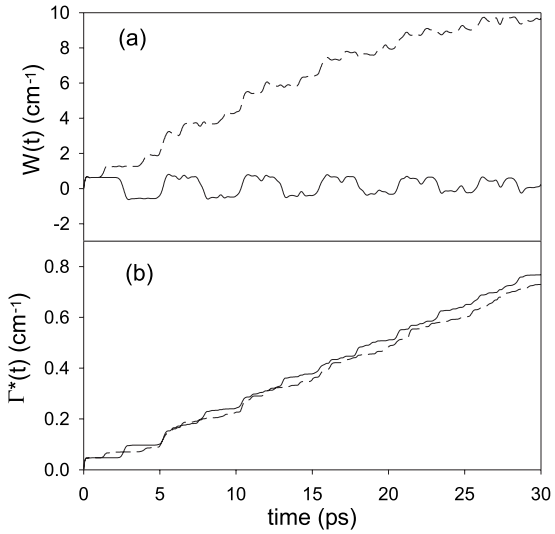

FIG. 7. Time evolution of (a) the transition rate and (b) the pure dephasing constant for $T=200$ K, $\chi=20$ pN, and $N=21$. Two dimer positions have been considered, i.e., $n_0=10$ (full line) and $n_0=5$ (dashed line).

increases by steps whose duration is equal to that of the steps characterizing $W(t)$. Although it increases according to time, the pure dephasing constant remains rather small in the short time limit. For instance, for $n_0=10$, the first step corresponds to $\Gamma^*(t)=0.05$ cm^{-1}, the second step to 0.1 cm^{-1}, and so on.

V. DISCUSSION

The numerical results have revealed that the coherent nature of the energy transfer between the two sites of the dimer is very sensitive to the finite size of the lattice. Indeed, the population difference first exhibits damped oscillations over a timescale called the coherent time. Then, it finally vanishes indicating that the equilibrium corresponds to a uniform energy distribution over the two sites of the dimer. However, the coherent time strongly depends on both the lattice size and the dimer position. For specific values of these parameters, the population difference decreases exponentially and rapidly vanishes. This feature indicates that the vibrational energy flow is characterized by a very short coherent time. By contrast, for other specific values of the lattice size and of the dimer position, a slowdown of the decoherence occurs. The coherent time is enhanced and $P(t)$ develops coherent oscillations over a significant time scale. It does not decay exponentially any more but it evolves by steps during which its amplitude experiences almost no damping. In addition, the occurrence of revivals has been observed for which $P(t)$ is amplified over specific time intervals. Nevertheless, both decoherence slowdown and revivals are limited so that the population difference finally reaches the equilibrium.

This surprising behavior originates in the evolution of the time dependent transition rate. When $W(t)$ exhibits a series of low amplitude steps alternatively positive and negative, $P(t)$ is clearly characterized by a significant coherent time. By contrast, when $W(t)$ develops a high amplitude sinelike shape, the coherent time is strongly reduced. Moreover, the numerical results have revealed that the pure dephasing constant increases by steps according to time. It is always positive so that $P(t)$ irreversibly tends to the equilibrium.

To discuss and interpret these observed features, let us recall that $W(t)$, $\Gamma^*(t)$, and $\Delta(t)$ are expressed in terms of the correlation function of the polaron-phonon coupling Hamiltonian $C_{\pm}(t)$ [Eq. (20)]. For the parameters considered in the present work, i.e., $\Omega_c \approx 100$ cm^{-1} and $\chi < 60$ pN, the main characteristic of these correlations is accounted by a second order expansion of the exponential function occurring in Eq. (20). The dynamical parameters are simply written in terms of $K(t)$ [see Eq. (21)] as

$$W(t) \approx 4\hat{\Phi}^2 \int_0^t dt_1 K(t_1)\cos(2\hat{\Phi}t_1),$$

$$\Gamma^*(t) \approx 2\hat{\Phi}^2 \int_0^t dt_1 K^2(t_1),$$

$$\Delta(t) \approx 2\hat{\Phi}^2 \int_0^t dt_1 K(t_1)\sin(2\hat{\Phi}t_1). \tag{24}$$

From a physical point of view, $K(t)$ defines a correlation function, i.e., $K(t) \propto \mathrm{Re}\langle \eta(t)\eta(0)\rangle_p$, where η is expressed in terms of the external displacements as

$$\eta = \sum_n [D^{-1/2}(n_0+1,n) + D^{-1/2}(n_0,n) - D^{-1/2}(n_0+2,n) - D^{-1/2}(n_0-1,n)]u_n. \tag{25}$$

The matrix $D(n,n')$ is the dynamical matrix whose eigenvalues Ω_p^2 specify the phonon frequencies. A numerical analysis has revealed that η describes a lattice deformation localized on the sites n_0 and n_1. Indeed, due to its coupling with the phonons, a polaron initially on n_0 realizes a hop on n_1 by exchanging energy with the phonon bath. This hop induces a lattice distortion involving the motion of the residues located in the vicinity of the dimer. This deformation evolves in time and it propagates along the lattice. Therefore, the correlation function $K(t)$ characterizes the memory of the lattice at time t of a deformation produced at the initial time.

The function $K(t)$ plays a key role in the present formalism. It allows us to understand the physical meaning of the dynamical parameters and to interpret the observed results. However, before considering the general situation, we shall first focus our attention on the simple case of a dimer embedded in an infinite lattice.

A. Dimer embedded in an infinite lattice

In a lattice with translational invariance, the phonons are the elementary excitations describing acoustic plane waves. Therefore, by generalizing Eq. (5), we first determine the coupling between the n_ith amide-I mode and the phonons with wave vector q (see, for instance, Ref. [7]). Then, this expression is inserted in Eq. (21) so that the high temperature limit of the correlation function $K(t)$ can be evaluated easily as

$$K(t) = K_0 \frac{J_1(\Omega_c t)}{\Omega_c t}, \tag{26}$$

where $K_0=(16k_BTE_B)/\Omega_c^2$ and J_1 is a Bessel function of the first kind.

Equation (26) reveals that $K(t)$ is strongly localized at the origin $t=0$. Starting from $K(0)=K_0/2$, it exhibits damped oscillations over a time scale of about $\tau_c=2/\Omega_c$ to finally vanish. In other words, the lattice experiences the memory of the initial distortion over a very short time scale. This time scale, called the phonon correlation time τ_c, measures the time required to the lattice deformation to leave the vicinity of the dimer. Indeed, after the initial creation of the lattice deformation, two acoustic wave packets are emitted on each side of the dimer. After a time of about τ_c, these wave packets have covered a distance of about a single lattice parameter. They have left the dimer region so that no correlation remains.

In α-helices, τ_c is shorter than the time governing the free evolution of a dimer ($\Omega_c \gg \hat{\Phi}$) so that the Markov approximation can be used. The dimer dynamics is governed by time independent dynamical parameters which are still given by

Eq. (24) in which the upper limit of the integrals is extended to infinity. By inserting Eq. (26) into Eq. (24), the dynamical parameters in the Markov limit are written as

$$W_0 = \frac{4\hat{\Phi}^2 K_0}{\Omega_c}\sqrt{1-\left(\frac{2\hat{\Phi}}{\Omega_c}\right)^2},$$

$$\Gamma_0^* = \frac{8\hat{\Phi}^2 K_0^2}{3\pi\Omega_c},$$

$$\Delta_0 = \frac{4\hat{\Phi}^3 K_0}{\Omega_c^2}. \tag{27}$$

Note that to account for its peaked nature, $K(t)$ can be represented by a Dirac function as $K(t)=K_0\tau_c\delta(t)$. Within this definition, the dynamical parameters are in very good agreements with their previous exact expressions [Eq. (27)] as

$$W_0 \approx \frac{4\hat{\Phi}^2 K_0}{\Omega_c},$$

$$\Gamma_0^* \approx \frac{\hat{\Phi}^2 K_0^2}{\Omega_c}, \tag{28}$$

where $\Delta_0 \approx 0$ in the limit $\Omega_c \gg \hat{\Phi}$.

With time independent coefficients, the TCLME Eq. (22) can be solved easily so that the resulting population difference is expressed as

$$P(t) = e^{-\gamma_0 t}\left[\cos(\Omega_0 t) - \frac{W_0}{2\Omega_0}\sin(\Omega_0 t)\right], \tag{29}$$

where

$$\gamma_0 = \Gamma_0^* + \frac{W_0}{2},$$

$$\Omega_0 = 2\hat{\Phi}\sqrt{1+\frac{\Delta_0}{\hat{\Phi}}-\left(\frac{W_0}{4\hat{\Phi}}\right)^2}. \tag{30}$$

Equation (29) reveals that $P(t)$ exhibits damped coherent oscillations with frequency Ω_0 and damping rate γ_0. This result corroborates recent calculations devoted to the energy relaxation in a nonlinear dimer coupled to a phonon bath [23]. Nevertheless, two main differences occur. Indeed, in Ref. [23] the coupling Hamiltonian ΔH has been linearized by assuming a sufficiently weak vibron-phonon interaction. As a result, by using a second order perturbation theory, it was shown that the damping rate γ_0 first scales linearly with respect to the small polaron binding energy E_B and second, is proportional to the square of the bare hopping constant Φ. In the present formalism, only the expansion of the correlation function of the polaron-phonon coupling has been performed. Consequently, the effective hopping constant $\hat{\Phi}$ occurs in the definition of the dynamical parameters instead of Φ. Moreover, this approach predicts a nonvanishing pure dephasing constant which yields an additional contribution to γ_0 proportional to E_B^2. The present theory is thus more general and it is not restricted to weak vibron-phonon coupling and low temperature.

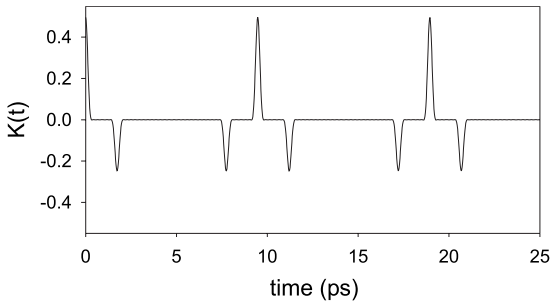

FIG. 8. Time evolution of $K(t)$ within the Debye model for $N=40$, $n_0=7$, $T=300$ K, and $\chi=30$ pN.

B. Dimer embedded in a finite size lattice

In a finite size lattice, $K(t)$ cannot be evaluated exactly. To overcome this difficulty, we consider the Debye model in which the phonon dispersion is neglected. The phonon frequency is thus assumed to scale linearly with the phonon wave vector as $\Omega_p=\Omega_c p\pi/(2L)$.

To proceed, we first express the vibron-phonon coupling $\delta\Delta_p=\Delta_{p0}-\Delta_{p1}$ in terms of the mean value of the dimer position $\hat{n}=(n_0+n_1)/2$. Then, this expression is inserted in Eq. (21) so that the high temperature limit of $K(t)$ is written as

$$K(t) = \frac{2K_0}{L}\sum_p \cos^2\left(\frac{p\pi}{2L}\right)\sin^2\left(\frac{p\pi\hat{n}}{L}\right)\cos\left(\frac{p\pi t}{T_0}\right), \tag{31}$$

where $T_0=2L/\Omega_c$ is the time required to an acoustic wave to cover the lattice. After some algebraic manipulations, the correlation function is expressed as

$$K(t) = \frac{K_0}{2}\left[g(t) - \frac{1}{2}g(t-T_1) - \frac{1}{2}g(t+T_1)\right], \tag{32}$$

where $T_1=4\hat{n}/\Omega_c$ and where $g(t)=f(t)+f(t-\tau_c)/2+f(t+\tau_c)/2$ is defined in terms of the function $f(t)$ written as

$$f(t) = \frac{1}{L}\cos\left(\frac{N\pi t}{2T_0}\right)\frac{\sin\left(\frac{L\pi t}{2T_0}\right)}{\cos\left(\frac{\pi t}{2T_0}\right)}. \tag{33}$$

In a finite size lattice, $f(t)$ is a periodic function whose period is equal to $2T_0$. It supports a high frequency low amplitude modulation and it exhibits a series of peaks whose amplitude is equal to one and which are centered on the discrete times $t_k=2kT_0$, with $k=0,1,2,\ldots$. The shape of $g(t)$ is very similar to that of $f(t)$. It shows a series of peaks centered on the same set of discrete times. The width of each peak is about $2\tau_c$ and its amplitude is almost equal to unity. Nevertheless $g(t)$ appears as a smooth function which does not support any high frequency low amplitude modulation. Consequently, as illustrated in Fig. 8, $K(t)$ is periodic with a period equal to $2T_0$. Over a single period, i.e., for $t_k \leqslant t$

$< t_{k+1}$, it shows a positive peak centered on t_k and two negative peaks located on the times t_k+T_1 and $t_{k+1}-T_1$, respectively. Although these peaks are characterized by a same width of about $2\tau_c$, the amplitude of the negative peaks is two times smaller than the amplitude of the positive peak.

In the limit N tends to infinity we have verified that Eq. (32) leads to the expression of the correlation function in an infinite lattice within the Debye model. Consequently, each peak exhibits the same shape as the peak characterizing $K(t)$ in a lattice with translational invariance. This feature allows us to generalize the Dirac peak approximation so that the correlation function simply reduces to

$$K(t) = K_0 \tau_c \sum_k \delta(t - t_k) - \frac{1}{2}\delta(t - t_k - T_1) - \frac{1}{2}\delta(t - t_{k+1} + T_1). \tag{34}$$

As in the infinite lattice, the initial creation of a local deformation yields two wave packets emitted on each side of the dimer. Therefore, a correlation remains over a time scale of about τ_c which characterizes the time required to the wave packets to leave the dimer region. This is the reason why $K(t)$ supports a peak at the origin $t=0$. At time $t \approx T_1/2$, one of the wave packets reaches a side of the lattice where it is reflected. It then propagates back to the dimer region and it interacts again with the dimer at time $t=T_1$. Because a dephasing occurs at the reflection, this wave packet is in phase opposition with the initial packets. Moreover, it shares half of the initial lattice distortion. Consequently, a negative peak appears in $K(t)$ whose amplitude is two times smaller than the amplitude of the initial peak. In the same way, the second negative peak in $K(t)$ originates in the interaction between the dimer and the second wave packet which has been reflected on the other side of the lattice. It thus occurs at the time $t=2T_0-T_1$. Finally, at time $T=2T_0$, each wave packet has experienced two reflections so that they reappear simultaneously in the dimer region with their initial phase. The lattice recovers its initial configuration and the correlation function exhibits a large positive peak equivalent to the peak at the origin.

The Debye approximation accounts for the main part of the behavior of the correlation function. When exact calculations are performed, the occurrence of peaks regularly distributed is observed. Nevertheless, due to the phonon dispersion, $K(t)$ exhibits a high frequency noise which modifies its periodic nature and favors the occurrence of a chaotic evolution in the long time limit. However, the analysis of the time integral of $K(t)$ reveals the presence of steps which are a characteristic of a periodic distribution of peaks. Since $K(t)$ occurs in the definition of the dynamical parameters through its integral, we conclude that the Debye model captures the main part of the physics.

In that context, the time dependent transition rate can be evaluated by inserting Eq. (34) into Eq. (24). It is expressed as

$$\begin{aligned} W(t) = W_0 \sum_k & 2(1 - \delta_{k,0}/2)\Theta(t - t_k)\cos(2\hat{\Phi}t_k) \\ & - \Theta(t - t_k - T_1)\cos[2\hat{\Phi}(t_k + T_1)] \\ & - \Theta(t - t_{k+1} + T_1)\cos[2\hat{\Phi}(t_{k+1} - T_1)], \end{aligned} \tag{35}$$

where W_0 is the value of the rate within the Markov approximation [Eq. (28)] and $\Theta(t)$ is the Heaviside function. In rather good agreement with our numerical results, Eq. (35) shows that the transition rate evolves by steps. A step occurs for each peak of the correlation function $K(t)$ so that $W(t)$ remains constant over a time scale specified by the delay between two consecutive peaks. When $t < T_1$, $W(t)$ is equal to W_0 which corroborates the short time limit of the rate illustrated in Figs. 3 and 7. Then, on the following steps, it increases or decreases. It can take either positive values, negative values, or vanish depending on the value of the phase factors $2\hat{\Phi}t_k$ and $2\hat{\Phi}(t_k \pm T_1)$. Note that as illustrated by the gray lines in Fig. 3, Eq. (35) yields a very good approximation for the time evolution of $W(t)$, especially in the short time limit. Nevertheless, rather small discrepancies occur mainly due to the phonon dispersion.

To understand this behavior in a simple way, let us consider the situation of a dimer located in the middle of the lattice. In that case, $T_1=T_0$ so that the two negative peaks over each period of $K(t)$ appear simultaneously. As a consequence, the time dependent rate evolves by step, each step occurring at the times 0, T_0, $2T_0, \ldots$ and so on. Therefore, let W_k denotes the value of the rate for $kT_0 \leqslant t < (k+1)T_0$. After performing straightforward calculations, W_k is written as

$$W_k = W_0 \frac{\cos[\hat{\Phi}T_0 + (2\hat{\Phi}T_0 + \pi)k]}{\cos(\hat{\Phi}T_0)}. \tag{36}$$

When $\hat{\Phi}T_0 = p\pi$, the rate reduces to $W_k=(-1)^k W_0$ so that it alternates periodically between W_0 and $-W_0$ in good agreements with the behavior observed in Fig. 3 and 7. When $\hat{\Phi}T_0$ slightly differs from $p\pi$, the rate exhibits a fast variation from one step to the next one and it alternates again between positive and negative values over a single period. When $\hat{\Phi}T_0$ increases again, the variations of the rate become more and more slow. The rate develops a high amplitude sinelike behavior as the one observed in Fig. 3. More precisely, when $\hat{\Phi}T_0=(p+1/2)\pi-\epsilon$, it is equal to $W_k=W_0 \sin[(2k+1)\epsilon]/\sin(\epsilon)$. Finally, when $\hat{\Phi}T_0=(p+1/2)\pi$, the rate increases form one step to the next one. It is always positive and reduces to $W_k=W_0(2k+1)$.

These results show that the time dependent transition rate exhibits different regimes depending on the value of the phase factor $\hat{\Phi}T_0$. To understand this feature, let us proceed as follows. We first assume the dimer in the eigenstate $|+\rangle$. Then, at time $t=0$, the dimer interacts with the phonons bath. Such a process occurs over a very short time scale of about τ_c so that it is as if the dimer-bath coupling was a delta pulse. The effect of this coupling is twofold. First, it creates a superimposition of $|+\rangle$ and $|-\rangle$, the weight of $|-\rangle$ being proportional to the coupling strength. Then, it induces a lattice distortion on the sites supporting the dimer. As the time increases, two wave packets are emitted on each side of the dimer. They experience a reflection and interact again with the dimer at time T_0. In the same time, the coherent superimposition has evolved freely. Consequently, this second interaction modifies the weight of the states $|\pm\rangle$. The weight of

$|-\rangle$ is reinforced by a phase factor $-\exp(2i\hat{\Phi}T_0)$ where the minus sign originates in the reflection. After that, the dimer evolves freely and the lattice distortion continues to propagate. A new interaction takes place at time $2T_0$ and so on. In other words, the reflections experienced by the lattice distortion confined in the finite size lattice lead to a series of couplings which modifies the nature of the superimposition. Each coupling occurring at time kT_0 contributes to a phase factor $(-1)^k \exp(2i\hat{\Phi}kT_0)$ in the weight of the state $|-\rangle$. Depending on the value of $\hat{\Phi}T_0$, this weight increases or decreases after each interaction which leads to the singular behavior of the corresponding transition rate discussed previously.

In a similar way, i.e., by inserting Eq. (34) into Eq. (24), the pure dephasing constant is expressed as

$$\Gamma^*(t) = \Gamma_0^* \sum_k (2 - \delta_{k,0})\Theta(t - t_k) + \frac{1}{2}\Theta(t - t_k - T_1) + \frac{1}{2}\Theta(t - t_{k+1} + T_1), \tag{37}$$

where Γ_0^* denotes its value within the Markov approximation [Eq. (28)]. The pure dephasing constant is always positive and it evolves by steps, as observed in Figs. 4 and 7. Although the results were not reported on the figures, we have verified that Eq. (37) yields a very good approximation for the time evolution of $\Gamma^*(t)$. As for $W(t)$, a step occurs for each peak of the correlation function $K(t)$ so that $\Gamma^*(t)$ is constant over a time scale separating two consecutive peaks. When the dimer lies in the middle of the lattice, each step occurs at times kT_0. Therefore, the value Γ_k^* of the dephasing constant over the range $kT_0 \leqslant t < (k+1)T_0$ reduces to $\Gamma_k^* = \Gamma_0^*(2k+1)$. In other words, the series of couplings experienced by the dimer due to the successive reflections of the lattice distortion yields an irreversible decay of the quantum coherence. Each interaction contributes to dephasing in a similar way so that the pure dephasing constant increases after each peak in the correlation function $K(t)$.

At this step, let us mention that the dynamical shift $\Delta(t)$ behaves similarly to the rate $W(t)$. However, it exhibits rather small values and it does not play a significant role in the understanding of the time evolution of the population difference. For that reason, its time evolution is not required and it will be disregarded in the present discussion.

According to the Debye model, the dynamical parameters evolve by steps. They remain constant over a timescale separating two consecutive interactions with the reflected lattice distortion created at time $t=0$. Consequently, let W_k, Γ_k^* and Δ_k denote the values of these parameters between two interactions. Over this time scale, the TCLME exhibits time independent parameters so that the corresponding population $P_k(t)$ is expressed as

$$P_k(t) = A_k^{(+)} e^{-\lambda_k (t - kT_0)} + A_k^{(-)} e^{-\lambda_k^* (t - kT_0)}, \tag{38}$$

where $\lambda_k = \gamma_k + i\Omega_k$ and where

$$\gamma_k = \Gamma_k^* + \frac{W_k}{2},$$

$$\Omega_k = 2\hat{\Phi}\sqrt{1 + \frac{\Delta_k}{\hat{\Phi}} - \left(\frac{W_k}{4\hat{\Phi}}\right)^2}. \tag{39}$$

Similarly to what append for a dimer in an infinite lattice, $P_k(t)$ shows coherent oscillations with frequency Ω_k. However, these oscillations are either damped or amplified, depending on the value of the constant γ_k. Indeed, although the pure dephasing constant is always positive and increases after each dimer-distortion interaction, the rate W_k can take positive and negative values depending on the phase factors $\hat{\Phi}T_0$ and $\hat{\Phi}T_1$. As a result, in a finite size lattice, the coherent nature of the energy exchange can be either enhanced or suppressed.

At this step, let us mention that this time discretization allows us to use a transfer matrix formalism to evaluate the amplitude of $P(t)$ after each peak of the correlation function $K(t)$. This approach, detailed in the Appendix for a dimer located at the center of the lattice, is based on the fact that both $P(t)$ and its first derivative are continuous functions. Consequently, $A_k^{(\pm)}$ is connected to $A_{k-1}^{(\pm)}$ through a transfer matrix which provides a rather good evaluation of the amplitude of the population difference.

To explain the observed behavior of the population difference, let us consider the case of a dimer occupying the center of the lattice. When $\hat{\Phi}T_0 = (p+1/2)\pi$, the rate increases from one step to the next one so that the damping constant reduces to $\gamma_k = \gamma_0(2k+1)$. Each dimer-distortion interaction favors the population transfer between the two dimer eigenstates which results in an enhancement of the quantum decoherence. The return to the equilibrium occurs over a very short time scale when compared with the coherent time characterizing a dimer in an infinite lattice. Since $T_0 = 2L/\Omega_c$, this regime takes place for specific value of the lattice size written as

$$N = \frac{(2p+1)\pi\Omega_c}{4\hat{\Phi}} - 1. \tag{40}$$

When $T=200$ K and $\chi=20$ pN, Eq. (40) reveals that for $N \approx 10$, 33, 55, 78, and 100, $P(t)$ exhibits a very short coherent time in a very good agreement with the numerical results displayed in Fig. 2.

In that regime, the Appendix clearly shows that the amplitude of $P(t)$ scales as $A_k^{(\pm)} \approx \exp(-\gamma_0 T_0 k^2)$. In a marked contrast with its exponential decay observed in an infinite lattice, the amplitude of the population difference decreases according to a Gaussian law. Such a feature is more pronounced in a small lattice in which the free evolution of the dimer is slow when compared with the time required to an acoustic wave to cover the lattice. Each time kT_0 can thus be viewed as a continuous variable, i.e., $t \approx kT_0$, so that the amplitude behaves as $A_k^{(\pm)} \approx \exp(-\gamma_0 \Omega_c t^2/2L)$ indicating that the coherent time scales $t_c(N) \approx L^{1/2}$.

When $\hat{\Phi}T_0=p\pi$, the rate W_k successively alternates between W_0 and $-W_0$ so that the damping constant reduces to $\gamma_k=\Gamma_0^*(2k+1)+(-1)^k W_0/2$. When $t<T_0$, $P(t)$ decays according to the damping rate γ_0 which characterizes the decoherence in an infinite lattice. However, when $T_0\leqslant t<2T_0$, the rate becomes negative so that $\gamma_1=\gamma_0+2\Gamma_0^*-W_0$. Therefore, for a sufficiently weak pure dephasing constant, γ_1 can become smaller than γ_0 indicating a slowdown of the decoherence. In addition, γ_1 can exhibit negative value leading to a revival of the coherence which is amplified over this time scale.

In other words, over the time intervals $[0,T_0]$, $[2T_0,3T_0]$,… the positive transition rate accounts for an enhancement of the population transfer between the dimer eigenstates which provides a fast quantum decoherence. The amplitude of $P(t)$ experiences a significant damping so that after the kth dimer-distortion interaction it scales as $A_k^{(\pm)}\approx\exp[-(\Gamma_0^* T_0 k^2+W_0 T_0/2)]$ for odd k values (see the Appendix). By contrast, over the time intervals $[T_0,2T_0]$, $[3T_0,4T_0]$,…, the invert process occurs. The dimer-distortion coupling tends to restore the population of the eigenstates and favors an increase of the coherence. However, this mechanism is limited by pure dephasing which leads to an irreversible decay of the population difference. Its amplitude just after time kT_0 reduces to $A_k^{(\pm)}\approx\exp(-\Gamma_0^* T_0 k^2)$ for even k values. Note that according to the relation $\hat{\Phi}T_0=p\pi$ this regime of decoherence slowdown occurs for specific value of the lattice size written as

$$N=\frac{2p\pi\Omega_c}{4\hat{\Phi}}-1. \tag{41}$$

When $T=200$ K and $\chi=20$ pN, Eq. (41) shows that for $N\approx 22$, 44, 67, and 89, $P(t)$ exhibits a rather large coherent time in a very good agreement with the numerical results displayed in Fig. 2.

In a general way, decoherence slowdown and revivals appear when Eq. (41) is almost satisfied. This feature is illustrated by the presence of rather large peaks in Fig. 2. It originates in the behavior of the rate W_k which varies rapidly from one step to the next one and takes regularly negative values. However, in the vicinity of Eq. (40), i.e., when $\hat{\Phi}T_0=(p+1/2)\pi-\epsilon$, we have shown that the rate behaves as a sine function whose frequency is proportional to ϵ. Since the amplitude of this function scales as $1/\epsilon$, the rate can take rather important negative values but for a large time of about T_0/ϵ. As a consequence, a revival can occur in $P(t)$ around $t\approx T_0/\epsilon$ as long as the pure dephasing constant is not too large. This feature is illustrated in Fig. 9 for which the vibron hopping constant has been reduced to $\Phi=4$ cm^{-1}. For $N=20$, $n_0=10$, $T=150$ K and $\chi=20$ pN, Fig. 9(a) shows that the damping rate $\gamma(t)$ exhibits negative values when t ranges between 29 and 49 ps. As a consequence, over this time scale, $P(t)$ is amplified so that its initial decay is compensated and a revival occurs for $t\approx 50$ ps. The full circles in Fig. 9(b) show that the transfer matrix formalism gives a rather good evaluation of the amplitude of $P(t)$. As shown in the Appendix, this amplitude reduces to $A_k^{(\pm)}\approx\exp(-S_k)$ with

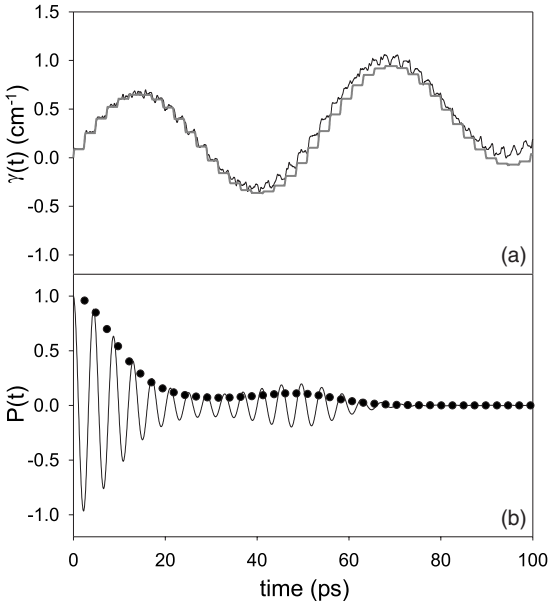

FIG. 9. Time evolution for (a) the damping rate $\gamma(t)$ and (b) the population difference for $N=20$, $n_0=10$, $T=150$ K, $\chi=20$ pN, and $\Phi=4$ cm^{-1}. Gray line in (a) describes the Debye model and full circles in (b) correspond to a theoretical calculation of $\hat{P}(\hat{t})$ (see the text).

$$S_k\approx\Gamma_0 T_0 k^2+\frac{W_0 T_0}{4\epsilon^2}[1-\cos(2k\epsilon)]. \tag{42}$$

The revival takes place for $k\approx\pi/\epsilon$ so that its amplitude scales as $A_k^{(\pm)}\approx\exp(-\Gamma_0 T_0/\epsilon^2)$ which illustrates the limitation induced by pure dephasing.

To conclude, let us mention that a similar discussion can be performed to describe the influence of the dimer position on the coherent nature of the energy flow. Because $T_1=4\hat{n}/\Omega_c$, the dimer position yields particular values for the phase factors $\hat{\Phi}T_1$ and $\hat{\Phi}(2T_0-T_1)$ which discriminate between different regimes for the transition rate. Therefore, an enhancement of the quantum decoherence can be observed, as well as a decoherence slowdown, as illustrated in Figs. 5 and 6.

VI. CONCLUSION

In this paper, a two-site Davydov model has been used to study the energy flow between two amide-I modes embedded in a finite size lattice of hydrogen-bounded peptide units. In such a lattice, the phonon dynamics is characterized by a recurrence time which accounts for the reflections experienced by the confined acoustic waves. Consequently, the energy transfer is clearly non-Markovian and it was described by using a TCLME for the dimer reduced density matrix. This equation involves three relevant parameters describing the effects of the dimer-phonon interaction. First, the time dependent transition rate accounts for the incoherent population transfer between the dimer eigenstates mediated by phonon exchange. Then, the pure dephasing constant describes the decoherence resulting from the energy fluctuation of each

dimer eigenstate. Finally the dynamical shift characterizes the time dependent energy shift of each eigenstates. Since these parameters are very sensitive to the finite size of the lattice, it has been shown that the coherent nature of the vibrational energy flow strongly depends on both the size of the lattice and the position of the dimer.

The origin of such dependence has been explained as follows. The dimer-phonon coupling favors the formation of a superimposition of the dimer eigenstates accompanied by a lattice distortion. This distortion propagates along the lattice so that two wave packets are emitted on each side of the dimer. However, because it is confined, the distortion is reflected so that it periodically propagates back to the dimer region leading to a series of dimer-distortion interactions. The influence of each interaction is twofold. First, it favors an irreversible decay of the coherence of the superimposition according to pure dephasing mechanism. Then, it modifies the weight of the dimer eigenstates according to phase factors resulting from both the free dimer evolution and the free phonon propagation between two successive interactions.

As a result, for specific values of the lattice size and of the dimer position, each interaction provides an efficient population transfer between the two eigenstates and enhances the decoherence. The vibrational energy flow is characterized by a very short coherent time. It decreases exponentially to rapidly vanish which indicates that the equilibrium corresponds to a uniform energy distribution over the two sites of the dimer. By contrast, for other specific values of the lattice size and of the dimer position, an interaction which favors a population transfer between the eigenstates is compensated by the next interaction which restores these populations. A slowdown of the decoherence takes place and the vibrational energy flow exhibits a rather large coherent time. Moreover, the occurrence of revivals has been observed which characterize an amplification of the coherence over a given time interval. Nevertheless, both decoherence slowdown and revivals are limited by pure dephasing which leads to an irreversible evolution to the equilibrium.

To conclude, let us mention that forthcoming works will be devoted to a generalization of the present approach to more realistic systems. First, the surprising features observed in the present study clearly involve the coherent nature of the confined phonons. However, in real proteins, we expected that both the anharmonicity and the inhomogeneous mass distribution in the amino acid sequence strongly modify such a coherent behavior. It would be wise to include these effects to quantify their influence on the amide-I dynamics. Then, the extension to a set of amide-I modes will provide a more accurate model to describe the energy flow in a finite size lattice. Finally, according to the original Davydov idea, nonlinear effects have to be included to characterize the behavior of multiquanta bound states known as the quantum equivalent to the Davydov soliton.

APPENDIX: TRANSFER MATRIX METHOD

When the dimer occupies the center of the lattice, the population difference for $kT_0 \leqslant t < (k+1)T_0$ is written as

$$P_k(t) = A_k^{(+)} e^{-\lambda_k (t-kT_0)} + A_k^{(-)} e^{-\lambda_k^* (t-kT_0)}, \tag{A1}$$

where $\lambda_k = \gamma_k + i\Omega_k$. Since both $P(t)$ and its first derivative are continuous for each discrete time kT_0, the transfer matrix formalism can be applied so that $A_k^{(\pm)}$ is connected to $A_{k-1}^{(\pm)}$ through the relation

$$\begin{pmatrix} A_k^{(+)} \\ A_k^{(-)} \end{pmatrix} = M_k \begin{pmatrix} A_{k-1}^{(+)} \\ A_{k-1}^{(-)} \end{pmatrix}. \tag{A2}$$

The matrix M_k is written in terms of the left-to-right ($\hat{t}_k$ and $\hat{r}_k$) and right-to-left (t_k and r_k) transmission and reflection coefficients as (see, for instance, Ref. [40])

$$M_k = \frac{1}{\hat{t}_k} \begin{pmatrix} \eta_k & \hat{r}_k \\ -r_k & 1 \end{pmatrix}, \tag{A3}$$

where $\eta_k = \hat{t}_k / \hat{t}_k^*$ and $t_k = |M_k| \hat{t}_k$. After straightforward calculations, these coefficients are expressed in terms of the relevant parameters of the problem as

$$\hat{t}_k = \frac{\lambda_k - \lambda_k^*}{\lambda_k - \lambda_{k-1}^*} e^{\lambda_{k-1}^* T_0},$$

$$\hat{r}_k = \frac{\lambda_{k-1}^* - \lambda_k^*}{\lambda_k - \lambda_{k-1}^*},$$

$$r_k = -\frac{\lambda_{k-1} - \lambda_k}{\lambda_k^* - \lambda_{k-1}} \eta_k,$$

$$t_k = \frac{\Omega_k}{\Omega_{k-1}} e^{-2\gamma_{k-1} T_0} \hat{t}_k. \tag{A4}$$

In that context, by applying Eq. (A2) recursively, the amplitudes $A_k^{(\pm)}$ are expressed in terms of $A_0^{(\pm)}$ through the generalized transfer matrix $M(k) = M_k M_{k-1} \ldots M_1$. Note that the initial condition $P(0) = 1$ and $J(0) = 0$ in Eq. (22) leads to the knowledge of the initial amplitudes $A_0^{(\pm)}$. The matrix $M(k)$ can be defined in terms of generalized transmission and reflection coefficients. Because it satisfies the fundamental multiplicative composition rule, the elementary coefficients can be evaluated step by step by using the rules

$$\hat{t}(2) = \frac{\hat{t}_2 \hat{t}_1}{1 - r_2 \hat{r}_1},$$

$$\hat{r}(2) = \frac{\hat{r}_2 + \hat{r}_1 \eta_2}{1 - r_2 \hat{r}_1},$$

$$r(2) = \frac{\eta_1 r_2 + r_1}{1 - r_2 \hat{r}_1},$$

$$t(2) = |M_2 M_1| \hat{t}(2). \tag{A5}$$

The amplitude of the population difference after the kth dimer-distortion interaction is characterized by the transmission coefficient $t(k)$ defined as

$$t(k) = \frac{\Omega_k}{\Omega_0} \exp\left(- \sum_{l=0}^{k-1} 2\gamma_l T_0 \right) \hat{t}(k). \tag{A6}$$

To evaluate $\hat{t}(k)$, we first neglect the variations of the frequency Ω_k from one step to another. Then, our numerical calculations have clearly shown that both the pure dephasing constant and the transition rate are rather small when compared with the dressed hopping constant. This feature allows us to neglect each reflection coefficient. Consequently, the composition of the transmission coefficients reduces to a multiplicative rule, i.e., $\hat{t}(k) \approx \hat{t}_k \hat{t}_{k-1} \ldots \hat{t}_1$, so that we obtain

$$t(k) \approx \exp\left(- \sum_{l=0}^{k-1} \gamma_l T_0 - ik\Omega_0 T_0 \right). \tag{A7}$$

By performing the sum in Eq. (A7), $A_k^{(\pm)}$ is finally expressed as

$$A_k^{(\pm)} \approx e^{-S_k}, \tag{A8}$$

where

$$S_k = \Gamma_0 T_0 k^2 + \frac{W_0 T_0}{2} \frac{1 - \cos[(2\hat{\Phi}T_0 + \pi)k]}{1 + \cos[2\hat{\Phi}T_0]}. \tag{A9}$$

[1] A. S. Davydov and N. I. Kisluka, Phys. Status Solidi A **59**, 465 (1973); Zh. Eksp. Teor. Fiz. **71**, 1090 (1976) [Sov. Phys. JETP **44**, 571 (1976)].
[2] D. W. Brown and Z. Ivic, Phys. Rev. B **40**, 9876 (1989).
[3] D. W. Brown, K. Lindenberg, and X. Wang, in *Davydov's Soliton Revisited*, edited by P. L. Christiansen and A. C. Scott (Plenum, New York, 1990).
[4] Z. Ivic, D. Kapor, M. Skrinjar, and Z. Popovic, Phys. Rev. B **48**, 3721 (1993).
[5] Z. Ivic, D. Kostic, Z. Przulj, and D. Kapor, J. Phys.: Condens. Matter **9**, 413 (1997).
[6] J. Tekic, Z. Ivic, S. Zekovic, and Z. Przulj, Phys. Rev. E **60**, 821 (1999).
[7] V. Pouthier, Phys. Rev. E **68**, 021909 (2003).
[8] V. Pouthier and C. Falvo, Phys. Rev. E **69**, 041906 (2004).
[9] C. Falvo and V. Pouthier, J. Chem. Phys. **123**, 184709 (2005).
[10] C. Falvo and V. Pouthier, J. Chem. Phys. **123**, 184710 (2005).
[11] D. V. Tsivlin and V. May, J. Chem. Phys. **125**, 224902 (2006).
[12] D. V. Tsivlin, H. Meyer, and V. May, J. Chem. Phys. **124**, 134907 (2006).
[13] J. Edler, R. Pfister, V. Pouthier, C. Falvo, and P. Hamm, Phys. Rev. Lett. **93**, 106405 (2004).
[14] J. Edler, V. Pouthier, C. Falvo, R. Pfister, and P. Hamm, in *Ultrafast Phenomena XIV*, edited by T. Kobayashi, T. Okada, T. Kobayashi, K. Nelson, and S. De Silvesti, Springer Series in Chemical Physics Vol. 79 (Springer, Berlin, 2005).
[15] I. G. Lang and Yu. A. Firsov, Sov. Phys. JETP **16**, 1293 (1962).
[16] V. M. Kenkre and P. Reineker, *Exciton Dynamics in Molecular Crystals and Aggregates* (Springer, Berlin, 1982).
[17] R. Silbey and R. W. Munn, J. Chem. Phys. **72**, 2763 (1979).
[18] R. W. Munn and R. Silbey, J. Chem. Phys. **83**, 1843 (1985).
[19] R. W. Munn and R. Silbey, J. Chem. Phys. **83**, 1854 (1985).
[20] B. J. West and K. Lindenberg, J. Chem. Phys. **83**, 4118 (1985).
[21] D. Brown, K. Lindenberg, and B. J. West, J. Chem. Phys. **83**, 4136 (1985).
[22] H. Dolderer and M. Wagner, J. Chem. Phys. **108**, 261 (1998).
[23] V. Pouthier, Physica D **221**, 13 (2006).
[24] R. Zwanzig, Lect. Theor. Phys. **3**, 106 (1961); Physica (Amsterdam) **30**, 1109 (1964); J. Chem. Phys. **33**, 1338 (1960).
[25] H. Mori, Prog. Theor. Phys. **33**, 423 (1965); **34**, 399 (1965).
[26] V. May and O. Kuhn, *Charge and Energy Transfer Dynamics in Molecular Systems* (Wiley-VCH Verlag, Berlin, 2000).
[27] L. Stryer, *Biochemistry*, 4th ed. (W. H. Freeman, New York, 1995).
[28] J. Wang and J. Feng, Protein Eng. **16**, 799 (2003).
[29] A. Pereverzev and E. Bittner, J. Chem. Phys. **125**, 104906 (2006).
[30] F. Shibata, Y. Takahashi, and N. Hashitsume, J. Stat. Phys. **17**, 171 (1977).
[31] C. Uchiyama and F. Shibata, Phys. Rev. E **60**, 2636 (1999).
[32] H. P. Breuer and B. Kappler, Ann. Phys. (N.Y.) **291**, 36 (2001).
[33] H. P. Breuer, B. Kappler, and F. Petruccione, Phys. Rev. A **59**, 1633 (1999).
[34] H. P. Breuer, J. Gemmer, and M. Michel, Phys. Rev. E **73**, 016139 (2006).
[35] M. Schroder, U. Kleinekathofer, and M. Schreiber, J. Chem. Phys. **124**, 084903 (2006).
[36] Y. Zhou, Y. Yan, and J. Shao, Europhys. Lett. **72**, 334 (2005).
[37] V. Capek and P. Chvosta, Czech. J. Phys. **40**, 585 (1990).
[38] V. Capek and P. Chvosta, Phys. Rev. A **43**, 2819 (1991).
[39] W. H. Press, S. A. Teukolsky, W. T. Vetterling, and B. P. Flannery, *Numerical Recipes in FORTRAN*, 2nd ed. (Cambridge University Press, Cambridge, UK, 1992).
[40] V. Pouthier and C. Girardet, Phys. Rev. B **66**, 115322 (2002).